Biological Psychiatry: GOS

Archival Report

Age-Related Alterations in Gray Matter Microstructure in Older People With Remitted Major Depression at Risk for Dementia

John A.E. Anderson, Neda Rashidi-Ranjbar, Arash Nazeri, Jordan A. Chad, Peter Zhukovsky, Benoit H. Mulsant, Nathan Herrmann, Linda Mah, Alastair J. Flint, Corinne E. Fischer, Bruce G. Pollock, Tarek K. Rajji, and Aristotle N. Voineskos, on behalf of the PACt-MD Study Group

ABSTRACT

BACKGROUND: Major depressive disorder (MDD) in late life is a risk factor for mild cognitive impairment (MCI) and Alzheimer's disease. However, studies of gray matter changes have produced varied estimates of which structures are implicated in MDD and dementia. Changes in gray matter volume and cortical thickness are macrostructural measures for the microstructural processes of free water accumulation and dendritic spine loss.

METHODS: We conducted multishell diffusion imaging to assess gray matter microstructure in 244 older adults with remitted MDD (n = 44), MCI (n = 115), remitted MDD+MCI (n = 61), or without psychiatric disorders or cognitive impairment (healthy control participants; n = 24). We estimated measures related to neurite density, orientation dispersion, and free water (isotropic volume fraction) using a biophysically plausible model (neurite orientation dispersion and density imaging).

RESULTS: Results showed that increasing age was correlated with an increase in isotropic volume fraction and a decrease in orientation dispersion index, which is consistent with neuropathology dendritic loss. In addition, this relationship between age and increased isotropic volume fraction was more disrupted in the MCI group than in the remitted MDD or healthy control groups. However, the association between age and orientation dispersion index was similar for all 3 groups.

CONCLUSIONS: The findings suggest that the neurite orientation dispersion and density imaging measures could be used to identify biological risk factors for Alzheimer's disease, signifying both conventional neurodegeneration observed with MCI and dendritic loss seen in MDD.

https://doi.org/10.1016/j.bpsgos.2023.08.018

Major depressive disorder (MDD) increases the risk of mild cognitive impairment (MCI), a precursor to Alzheimer's disease (AD) (1,2). This risk remains even when MDD is in remission (3–6). The neural markers of AD risk in individuals with remitted MDD (rMDD) remain unclear (7–10). Cortical thickness and volume are lagging indicators of neuronal disruption, and microstructural changes to neurons and neurites, such as age-related decreases in dendritic arborization and spine density, precede macrostructural changes (11–16). Advances in acquisition and modeling of diffusion-weighted imaging (DWI) have allowed insight into the microstructure of gray and white matter in vivo. More sensitive measures of cortical microstructure may serve to uncover proxies for dementia risk.

Despite mixed findings on gray matter changes in MDD across age groups (17,18), a recent comprehensive meta-analysis pointed out changes in frontoparietal and corticolimbic regions in patients with MDD (19). Our research found no alterations in cortical macrostructure or standard white matter DWI measures in individuals with rMDD compared with individuals without MDD (10,20). However, neurite measures could offer a better indicator of postmortem neuritic changes (21–23). While gray matter neurite changes have been investigated in dementia and MCI (21,24), we are unaware of such studies involving patients with MDD.

Neurite orientation dispersion and density imaging (NODDI) (25) mathematically describes neurites as water diffusing along with bundles of sticks varying by density (neurite density index [NDI]) and degree of dispersion (orientation dispersion index [ODI]). In gray matter, high ODI suggests greater dendritic complexity, while in white matter, it implies disorganized fiber bundles and cellular debris accumulation (26,27). NODDI and similar models account for isotropic diffusion (isotropic volume fraction [fISO]), which is free water, in each voxel. We have found that fISO microstructural changes are strongly correlated with cortical tau as measured by positron emission tomography (28) in older individuals who are healthy, have MCI, or have AD. Moreover, increased tau and fISO were associated with cognitive decline, with fISO being more linked to tau

ISSN: 2667-1743

presence than cortical thickness, which is typically considered the prime indicator of cortical atrophy and tau-related neurodegeneration (29). These findings suggest that microstructural properties such as fISO may be more reflective of AD pathology and could help detect early subtle changes that are predictive of AD.

In this context, we conducted a NODDI analysis in a large sample of older adults with rMDD, MCI (our sample included both amnestic MCI [aMCI] and nonamnestic MCI [naMCI]), or rMDD+MCI, and nonpsychiatric healthy control (HC) participants. The rationale for testing at-risk groups, including rMDD (vs. active MDD), has been published recently (30). First, we examined the relationship between age and the NODDI measures ODI, NDI, and fISO in the total sample to estimate an overall age effect. Then we examined how this relationship was maintained or disrupted in the various diagnostic groups. Given our recent findings of a relationship between tau and fISO, we hypothesized that age-related associations with NODDI measures would be somewhat disrupted in people with rMDD or MCI and most disrupted in people with rMDD and MCI.

METHODS AND MATERIALS

Participants

Magnetic resonance imaging (MRI) data were acquired in the context of an ongoing clinical trial called PACt-MD (Prevention of Alzheimer's Dementia With Cognitive Remediation Plus Transcranial Direct Current Stimulation in Mild Cognitive Impairment and Depression), which was approved by the Centre for Addiction and Mental Health Research Ethics Board (ClinicalTrials.gov Identifier: NCT02386670) (30). Of 387 participants, 321 completed an MRI, and 244 were included in this analysis (Figure 1). The methods and sample of PACt-MD have been described in detail previously (10,30). Briefly, all participants provided written informed consent and underwent a comprehensive baseline assessment, including cognitive testing. All data presented here, including the MRI data, are from the baseline assessments at the start of the clinical trial and thus represent cross-sectional comparisons among groups.

The cognitive battery included the tests that are described herein. To assess working memory, an inverse efficiency measure (reaction time/accuracy) was derived from 2- and 3-back versions of the n-back task (31). Sustained attention was assessed with d prime scores from the continuous performance task (32). In addition, *z* scores were calculated from the total number of correct items on the Paced Auditory Serial Addition Test, which captures participants' speed, ability to process auditory information, and capacity for calculation (33). The number of errors subtracted from the total number of completed items on the Digit Symbol Substitution Test (coding) was used to measure participants' associative learning (34). Attention and task switching were measured by the Trail Making Test, where the ratio of Trails B/A scores was taken into account (35). The color/word switching task (Stroop) produced corrected accuracy, which was then *z* scored to assess selective attention, processing speed, and inhibitory control (36). The Performance Assessment of Self-Care Skills was used to measure overall functional status as indicated by the total number of correct items from the shopping task (37). The semantic, or category, test (fluency) used the total number of correct items to indicate vocabulary size, lexical access, and speed of processing (38). Performance on the Brief Visuospatial Memory Test, which assessed visuospatial learning and memory, was judged by summing raw scores from trials 1 to 3 (39). Similarly, for the California Verbal Learning Test, raw free recall scores across trials 1 to 5 were summed for an assessment of verbal learning and memory (40). Lexical retrieval abilities were measured using the total number of correct items on the Boston Naming Test (41). Finally, overall executive and visuospatial functioning was evaluated using the total score on the clock task (42). Baseline diagnoses were established in a clinical consensus conference in which the results of the cognitive testing and all other available information were considered (30,43).

The participants who were included in this analysis consisted of 44 participants 65 years and older with rMDD, 61 participants 65 years and older with rMDD+MCI, and 115 participants 60 years and older with MCI. In this analysis, we further divided the MCI group into aMCI and naMCI groups (44), defining aMCI as MCI with impairment in memory on the Brief Visuospatial Memory Test or California Verbal Learning Test. In addition, PACt-MD recruited an HC comparator group of older adults without a history of psychiatric disorders or cognitive impairment; 24 control participants with usable MRI data were included in this analysis. Characteristics of the 244 participants included in the analysis are presented in Table 1.

MRI Acquisition

As described previously (10,20), participants from the PACt-MD study were all scanned on the same 3T GE Echospeed (General Electric) research-dedicated scanner at the Centre for Addiction and Mental Health. Whole-brain DWI including 30 gradient directions with b = 1000 s/mm^2, 33 gradient directions with b = 3000 s/mm^2, and 5 baseline scans with b = 0 s/mm^2 was performed using an echo-planar imaging sequence with a dual spin-echo option to reduce eddy current–related distortions (echo time [$TE_{b1000/b3000}$] = 110 ms, repetition time [TR_{b1000}] = 1100 ms, [TR_{b3000}] = 1200 ms; field of view = 25.6 cm; 128 × 128 matrix; 2.0 mm isotropic voxels; no gap; 81 slices). Axial slices were acquired parallel to the anterior commissure–posterior commissure line covering the whole brain. T1-weighted MRIs were acquired as sagittal 3-dimensional fast spoiled gradient-echo images (TE = 3 ms; TR = 6.7 ms; inversion time = 650 ms; flip angle 8°, field of view = 24 cm; number of excitations = 1, with 0.9 mm isotropic voxels, no gap, 81 slices). To correct for susceptibility-induced distortions, we also acquired 2 magnitude images with TE = 6.5 ms and TE = 8.5 ms, TR = 1000 ms, and field of view = 22 cm using an interleaved slice order, 64 × 64 matrix from which we estimated participant-specific field maps.

Image Preprocessing and Analysis

Diffusion-weighted b1000 and b3000 runs, along with the b0 runs, were concatenated and denoised with the MRtrix3 dwidenoise command (see Figure 2 for an overview of preprocessing steps). b0 images were used for brain extraction using the brain extraction toolbox from the FMRIB Software Library (FSL version 5.0.10) (45,46).

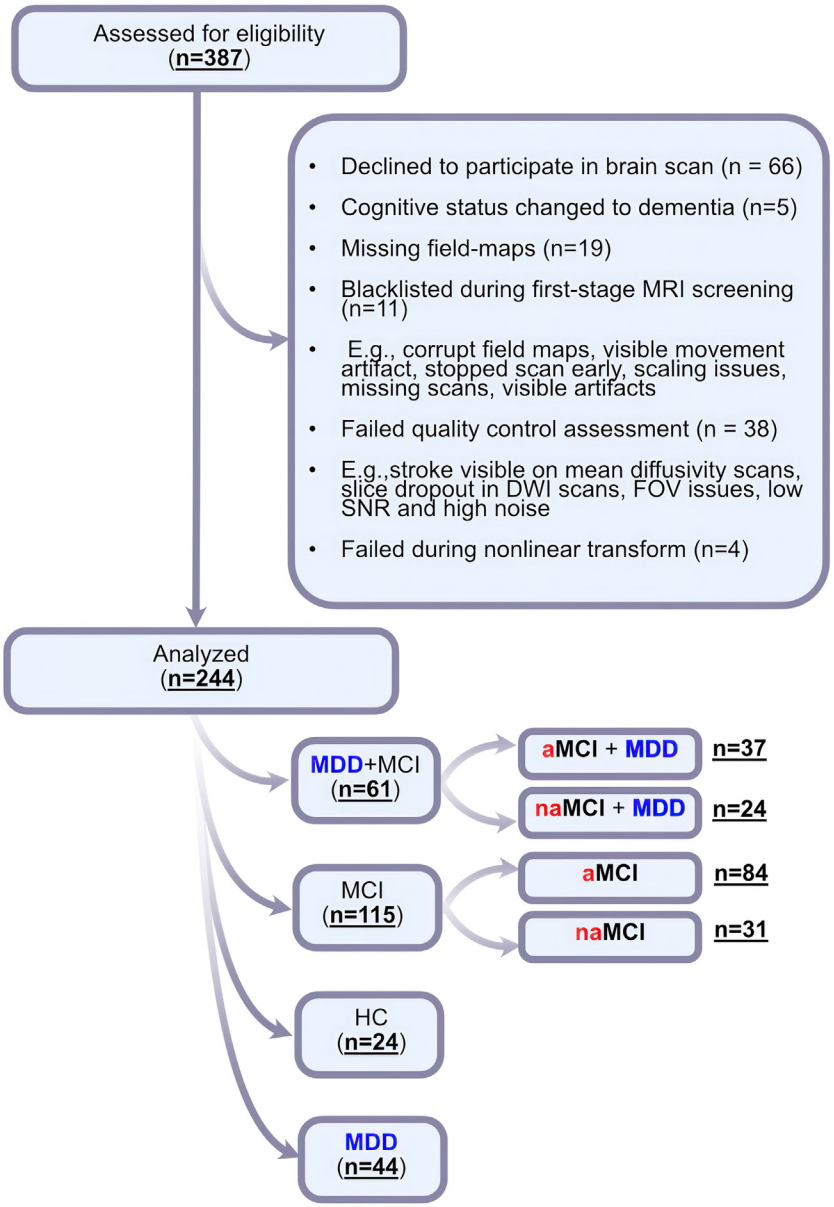

Figure 1. CONSORT (Consolidated Standards of Reporting Trials) diagram. aMCI, amnestic MCI; DWI, diffusion-weighted imaging; FOV, field of view; HC, healthy control; MCI, mild cognitive impairment; MDD, major depressive disorder; MRI, magnetic resonance imaging; naMCI, nonamnestic MCI.

Next, we corrected the DWI data for motion, eddy current–induced and susceptibility-induced distortions, and artifacts using an acquired field map in a single step using EDDY (FSL version 5.0.10) (45,46). NODDI measures were estimated using the microstructure diffusion toolbox (47,48). The measures of interest were the NDI, ODI, and fISO. We also used FSL's *dtifit* algorithm to estimate fractional anisotropy to estimate the pseudo-T1 images.

Gray Matter–Based Spatial Statistics

We used the gray matter–based spatial statistics (49–51) to estimate gray matter cortical skeletons minimizing partial voluming from white matter and extraparenchymal cerebrospinal fluid into core gray matter. This approach also avoids applying a Gaussian blur across anatomical boundaries. Pseudo-T1 images were estimated in a 3-step process outlined in Nazeri *et al.* (50,51). Briefly, we derived a gray matter probability map for each participant by generating a binary whole-brain mask and subtracting regions of likely cerebrospinal fluid (derived from the NODDI fISO map) and white matter (derived from a 2-tissue class segmentation of fractional anisotropy using Atropos). Tissue contrasts were enhanced by multiplying fISO maps by 0, gray matter by 1, and white matter by 2. These images were summed and used to generate a study-specific template using the

Table 1. Characteristics of the 244 Participants

	Amnestic		Nonamnestic			
Variable	aMCI, *n* = 84	aMCI+MDD, *n* = 37	HC, *n* = 24	naMCI, *n* = 31	naMCI+MDD, *n* = 24	MDD, *n* = 44
Sex at Birth						
Female	46 (55%)	24 (65%)	15 (62%)	18 (58%)	19 (79%)	31 (70%)
Male	38 (45%)	13 (35%)	9 (38%)	13 (42%)	5 (21%)	13 (30%)
Age, Years	73 (±7.6)	72 (±4.5)	70 (±6.1)	72 (±6.8)	71 (±4.4)	71 (±5.1)
Education, Years[a]	5.6 (±1.3)	5.5 (±1.2)	6.2 (±0.88)	5.9 (±1.0)	6.0 (±0.86)	6.0 (±1.2)
MMSE Score	27 (±3.4)	28 (±1.8)	28 (±6.0)	28 (±1.5)	29 (±1.2)	29 (±4.5)
MoCA Score	23 (±3.4)	24 (±2.6)	28 (±1.4)	25 (±2.0)	26 (±2.8)	28 (±2.0)
MADRS Score	3.6 (±2.9)	4.5 (±3.1)	1.0 (±1.5)	3.8 (±2.7)	5.0 (±3.8)	4.6 (±3.1)
WRAT Reading Score	62 (±5.2)	63 (±5.0)	66 (±3.7)	64 (±4.1)[b]	66 (±3.9)	66 (±3.6)

Values are presented as mean (±SD) or *n* (%).

aMCI, amnestic mild cognitive impairment; HC, healthy control; MADRS, Montgomery–Åsberg Depression Rating Scale; MDD, major depressive disorder; MMSE, Mini-Mental State Examination; MoCA, Montreal Cognitive Assessment; naMCI, nonamnestic MCI; WRAT, Wide Range Achievement Test.

[a]Education was measured as follows: 1, less than 7th grade; 2, junior high (9th grade); 3, partial high school (10th or 11th); 4, high school graduate; 5, partial college (at least one year); 6, college education; 7, graduate degree.

[b]WRAT Reading score data are missing for one (3.2%) naMCI participant.

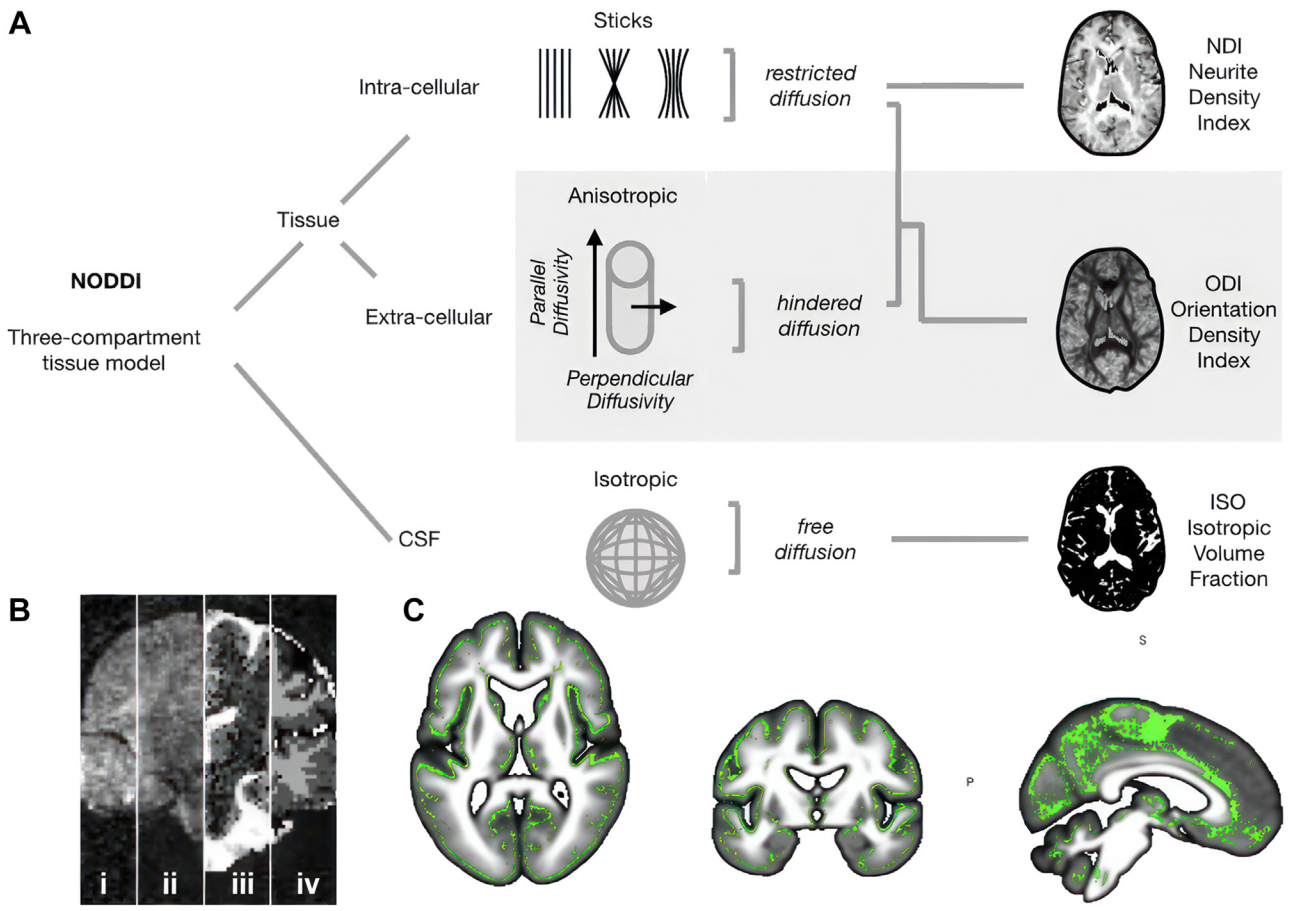

Figure 2. Methods overview. Panel **(A)** describes the neurite orientation dispersion and density imaging (NODDI) model and derived measures (neurite density index [NDI], orientation dispersion index [ODI], and isotropic volume fraction [fISO]). Panel **(B)** provides a brief visual overview of the preprocessing steps and gray matter–based spatial statistics and shows **(i)** raw diffusion-weighted imaging data, **(ii)** denoised EDDY/motion/susceptibility-corrected data, **(iii)** NODDI model fISO estimate, and **(iv)** pseudo-T1 image estimated via the gray matter–based spatial statistics algorithm. Panel **(C)** shows the group-derived gray matter skeleton used to constrain all analyses. CSF, cerebrospinal fluid.

buildtemplateparallel.sh script from the Advanced Normalization Tools toolbox. Nonlinear transforms from the previous step moved participant-specific estimates of gray matter and NODDI derivatives into template space. We used a skeletonization algorithm on the averaged gray matter map from all participants to achieve a consistent gray matter representation. This algorithm preserves only the local maxima perpendicular to the white matter tracts. Each participant-specific diffusion measure was projected onto this skeleton following tract-based spatial statistics (52). The procedure and scripts used can be found at https://github.com/arash-n/GBSS.

We visually checked the corrected 4-dimensional diffusion volume and verified the success of the brain extraction. We also examined the color-encoded maps of the primary eigenvector (V1) and, finally, residuals from the tensor fit (i.e., sum-of-squared-error maps) to ensure that no imaging artifacts remained following correction.

Statistical Analysis

Data were analyzed with behavioral partial least squares (PLS) using the MATLAB (version 2021b; The MathWorks, Inc.) implementation distributed by the Rotman Research Institute (53). PLS is a multivariate approach similar to principal component analysis (PCA) (54). Whereas PCA is an unsupervised method that decomposes variables into a set of components ranked from the highest to the least amount of explained variance, behavioral PLS attempts to maximize the explained variance in the *Y* matrix (behavior) in relation to the *X* matrix (brain data). Here, age was the behavioral variable [see, e.g., Figure 4 in (54)]. See the Supplement for additional details on the PLS method.

Before entering NODDI maps into PLS, each was residualized using the *fsl_glm* command (FSL version 5.0.10) (45,46). Nuisance variables included sex, number of years of education, and the first principal component of a PCA using quality control estimates (e.g., residual noise, average contrast-to-noise ratio, average signal-to-noise ratio, percent outliers, relative motion, and absolute motion) from eddyqc Quality Assessment for DMRI (55) and MRtrix (56). Residual noise, motion, and percent outliers loaded positively on the component score, while average signal-to-noise ratio and contrast-to-noise ratio loaded negatively, suggesting that the component tracked overall scan quality. Age was a covariate of interest and was entered directly into the behavioral PLS model.

To analyze differences among our groups (HC, MDD, aMCI, naMCI, MDD+aMCI, MDD+naMCI) in behavioral PLS results, we used bootstrap replicates for brain-behavior correlations, subtracted them for each pairwise comparison, and fit a 95% CI to the resulting distribution. Groups with 95% confidence bounds excluding 0 were deemed significantly different (see embedded tables in Figures 4 and 5). We also included Cohen's *d* estimates, computed from the bootstrap replicates, in the figures for easier interpretation of the importance of group differences.

Three behavioral PLS analyses were run with age as a predictor. The first analysis incorporated all 3 modalities (NDI, fISO, and ODI) to see how they varied by age. The second analysis explored whether the relationship between fISO and age differed by diagnosis. The third analysis replicated this approach of exploring the relationship between a brain measure and age by diagnosis, but with ODI as the outcome measure for the brain. The first analysis showed that NDI did not vary with age, and therefore, we did not do a separate analysis for this modality.

To mitigate effects of multicollinearity and multiple comparisons, we applied PCA to reduce dimensions of 12 cognitive scores. We used the MICE package in R (https://cran.r-project.org) for estimating missing behavioral data with chained equations before dimension reduction. The Paced Auditory Serial Addition Test had the highest missingness, at 17%, followed by the 3-back at 14%. Results remained consistent when these variables were excluded; therefore, we have presented the complete set of results. All other variables had <10% missing values across participants.

RESULTS

Results from the PLS analyses are presented in Figures 3–6 and Tables S1–S3.

Global Age Effects on NODDI Measures

We ran an initial behavioral PLS model across all groups to observe overall age-related changes in NODDI measures (Figure 3 and Table S1 for clusters) and replicate Nazeri *et al.* (50). A single latent variable was significant ($p < .001$) and explained 63.2% of the cross-block covariance.

As can be seen in Figure 3, age-related changes in NODDI measures were broadly distributed throughout the cortical and subcortical gray matter, with the strongest expression in the caudate nuclei. These changes can broadly be described as a steep increase in fISO ($r = 0.63$, 95% CI [0.54–0.71]) and a decline in ODI ($r = -0.60$, 95% CI [−0.68 to −0.52]). NDI was comparatively stable across the age range, and the correlation with age did not reliably differ from 0 ($r = 0.14$, 95% CI [−0.04 to 0.28]). For this reason, the rest of the analyses focused on group differences in ODI and fISO.

Group Differences in ODI-Age Relationships

Our first analysis examined how ODI changed with age in each diagnostic group.

Figure 4 shows that the relationship between ODI and age differs by diagnostic group (Table S2 for clusters). A single latent variable was significant ($p < .001$) and explained 28.6% of the cross-block covariance. The negative spatial pattern, indicating regions in which ODI decreased with increasing age, is constrained to the bilateral caudate nuclei, posterior visual cortex, and posterior cingulate cortex. Opposite results were observed in the cerebellum (i.e., ODI increases with age). Overall, Figure 4 shows a graduated change in ODI with age across groups, from the HC group, which shows the largest age-related changes, to the rMDD group, which shows the least. This pattern is broadly consistent, with individuals with naMCI being most sensitive to age-related changes, while changes in individuals with amnestic impairments seem less tightly coupled to age. Interestingly, the rMDD group was similar to the aMCI group in terms of this measure. The HC group ($r = 0.93$, 95% CI [0.87–0.96]) showed stronger age-related changes in ODI than the rMDD ($r = 0.60$, 95% CI [0.26–0.79]), aMCI ($r = 0.69$, 95% CI [0.56–0.80]), and rMDD+aMCI ($r = 0.58$, 95% CI [0.34–0.74]) groups. The 2 groups that showed the fewest age-related changes in ODI, the

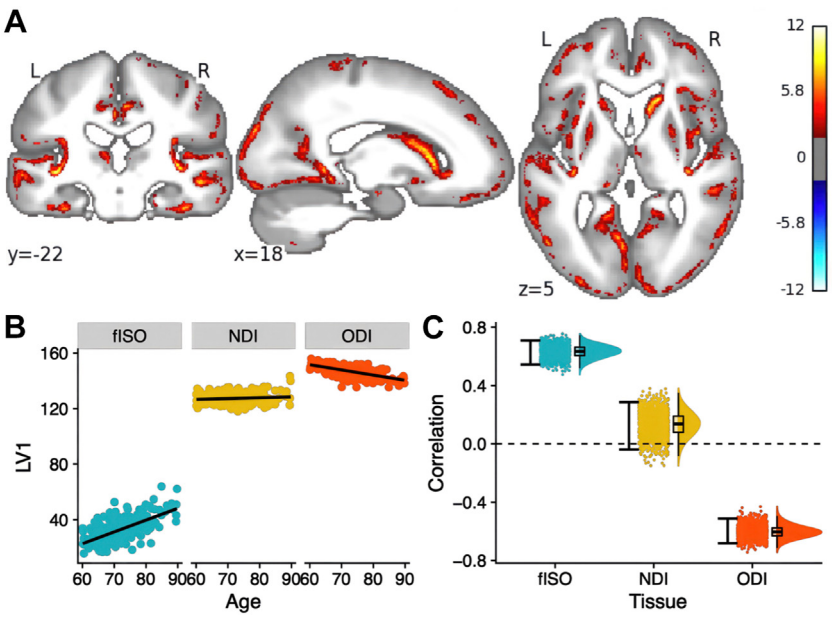

Figure 3. Neurite orientation dispersion and density imaging gray matter measures by age. Panel **(A)** is a bootstrap ratio image that represents the loadings of each voxel on the latent partial least squares variable. Bootstrap ratios are thresholded at ±2, showing regions where voxels are reliably different from 0 (roughly equivalent to $p < .05$). The spatial map should be interpreted alongside the correlations with age represented in **(B)** and **(C)**. Panel **(B)** shows the correlations between age (x-axis) and brain scores (y-axis). Brain scores represent the extent to which all participants within each condition load onto the brain map. Panel **(C)** presents the correlations shown in panel **(B)** as bootstrapped distributions with 95% CIs to accentuate the differences in correlations with age. Thus, panel **(A)** voxels with higher intensity showed a strong positive relationship with isotropic volume fraction (fISO), a negative relationship with the orientation dispersion index (ODI), and no clear relationship with neurite density index (NDI). L, left; LV, latent variable; R, right.

rMDD and rMDD+aMCI groups, were also each reliably different from the naMCI group (r = 0.89, 95% CI [0.80–0.95]).

Group Differences in fISO-Age Relationships

Figure 5 reveals that the impact of age on fISO produces a sharper divide between the HC group, the rMDD group, and the aMCI and naMCI groups (see Table S3 for clusters). A single latent variable was significant ($p < .001$) and explained 30.5% of the cross-block covariance. The spatial pattern associated with age-related changes in fISO localized to the bilateral frontal cortices, right caudate nucleus, right hippocampus, posterior cingulate cortex, and cerebellum. As with the

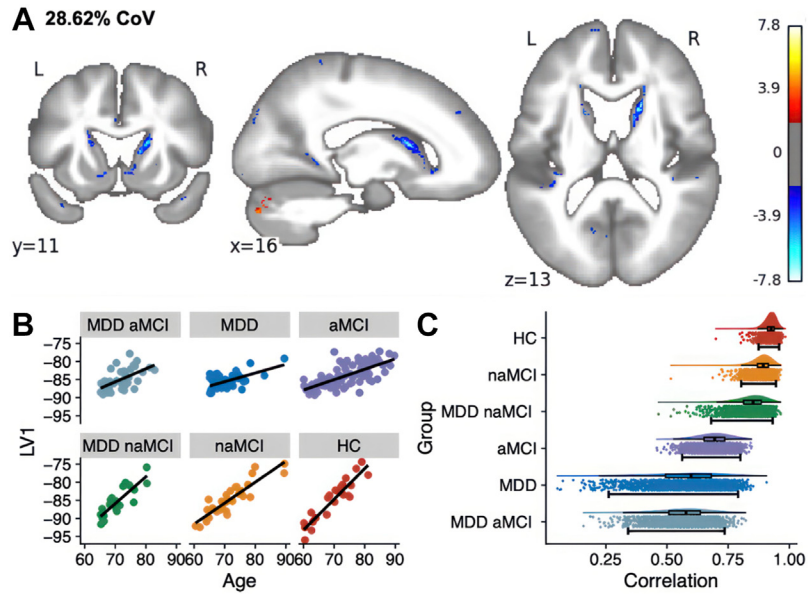

D

	2.5%	50%	97.5%	d
HC vs MDD	0.12	0.33	0.68	**2.38**
HC vs aMCI	0.12	0.22	0.37	**3.47**
HC vs naMCI	-0.04	0.03	0.13	0.83
HC vs MDD aMCI	0.18	0.35	0.58	**3.57**
HC vs MDD naMCI	-0.02	0.07	0.24	1.35
MDD vs aMCI	-0.46	-0.10	0.14	-0.74
MDD vs naMCI	-0.66	-0.29	-0.07	**-2.05**
MDD vs MDD aMCI	-0.38	0.02	0.33	0.04
MDD vs MDD naMCI	-0.62	-0.25	0.01	-1.67
aMCI vs MDD aMCI	-0.10	0.13	0.37	1.09
aMCI vs MDD naMCI	-0.31	-0.15	0.04	-1.73
naMCI vs MDD aMCI	0.14	0.32	0.55	**3.05**
naMCI vs MDD naMCI	-0.07	0.04	0.21	0.71

Figure 4. Relationship between orientation dispersion index (ODI) and age by diagnostic group. Panel **(A)** shows the spatial map with reliable bootstrap ratio values (thresholded at ±2). Panels **(B)** and **(C)** show the correlation results. Panel **(B)** shows the raw correlations between age and brain scores for each group, and panel **(C)** shows the bootstrapped median correlation with a 95% confidence estimate. Panel **(D)** presents a table of group differences derived from the bootstrap replicates with 95% confidence bounds and a Cohen's d estimate. Thus, in panel **(B)**, latent variable 1 (LV1) summarizes the ODI data, to which the voxels shown in blue in panel **(A)** make the most robust contributions. Older age was associated with lower ODI in the bilateral caudate nuclei and higher ODI in the cerebellum. aMCI, amnestic MCI; CoV, covariance; HC, healthy control; L, left; MCI, mild cognitive impairment; MDD, major depressive disorder; naMCI, nonamnestic MCI; R, right.

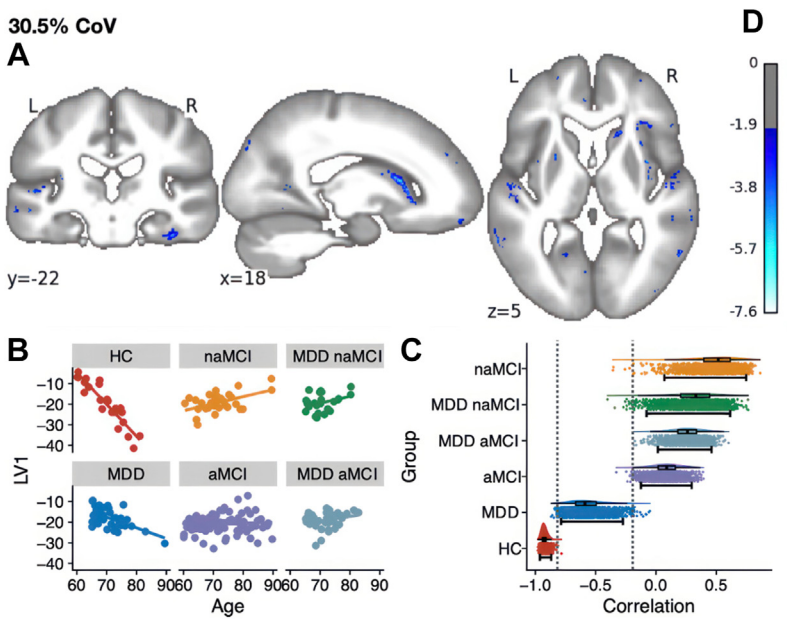

D

	2.5%	50%	97.5%	d
HC vs MDD	-0.67	-0.34	-0.13	**-2.53**
HC vs aMCI	-1.21	-1.01	-0.78	**-8.39**
HC vs naMCI	-1.67	-1.44	-1.01	**-8.75**
HC vs MDD aMCI	-1.40	-1.18	-0.92	**-9.42**
HC vs MDD naMCI	-1.54	-1.25	-0.86	**-6.73**
MDD vs aMCI	-0.97	-0.66	-0.29	**-3.51**
MDD vs naMCI	-1.44	-1.09	-0.56	**-4.69**
MDD vs MDD aMCI	-1.15	-0.84	-0.44	**-4.39**
MDD vs MDD naMCI	-1.26	-0.89	-0.41	**-3.93**
aMCI vs MDD aMCI	-0.50	-0.18	0.16	-1.02
aMCI vs MDD naMCI	-0.62	-0.24	0.20	-1.10
naMCI vs MDD aMCI	-0.23	0.25	0.60	1.18
naMCI vs MDD naMCI	-0.31	0.18	0.64	0.75

Figure 5. Relationship between isotropic volume fraction (fISO) and age by diagnostic group. Panel **(A)** shows the spatial map with reliable bootstrap ratio values (thresholded at ±2). Panels **(B)** and **(C)** show the correlation results. Panel **(B)** shows the raw correlations between age and brain scores summarizing fISO in the regions highlighted in panel **(A)** for each group, and panel **(C)** shows the bootstrapped median correlation with a 95% confidence estimate. Panel **(D)** presents a table of group differences derived from the bootstrap replicates with 95% confidence bounds and a Cohen's *d* estimate. Thus, in panel **(B)**, latent variable 1 (LV1) summarizes the fISO data, to which the voxels shown in blue in panel **(A)** make the most robust contributions. aMCI, amnestic MCI; CoV, covariance; HC, healthy control; L, left; MCI, mild cognitive impairment; MDD, major depressive disorder; naMCI, nonamnestic MCI; R, right.

analysis of ODI, the relationship between fISO and age was strongest in the HC group ($r = -0.93$, 95% CI [−0.96 to −0.87]). This relationship was present but attenuated in the rMDD group ($r = -0.59$, 95% CI [−0.79 to −0.27]). Thus, there was an increase in fISO with age in both these groups. In contrast, all MCI groups (with or without rMDD) showed a much weaker association between age and fISO, with an overall correlation of $r = 0.27$, 95% CI (−0.08 to 0.68), suggesting that the relationship between age and neurodegeneration/atrophy was disrupted. The age-fISO relationship was stronger in the HC group than in the rMDD group. Furthermore, the age-fISO relationship was stronger in the HC and rMDD groups than in any of the MCI groups and did not differ in any of the MCI groups, suggesting that age had a similarly weak influence in these groups.

Brain-Behavior Relationships

The first principal component for cognitive performance explained 35.6% of the variance and captured general cognitive performance across a range of memory and executive function tasks (Figure 6 A, B). This first principal component was negatively predicted by fISO ($F_{1,243} = 44.9$, $p = 1.454 \times 10^{-10}$, adjusted $r^2 = 0.15$) and positively predicted by ODI ($F_{1,243} = 29$, $p = 1.743 \times 10^{-7}$, adjusted $r^2 = 0.10$).

DISCUSSION

Overview of Findings

We investigated the associations among gray matter ODI, NDI, fISO, age, diagnostic group, and cognitive performance. As hypothesized, rMDD and MCI disrupted the relationship between age and gray matter microstructure, although rMDD+MCI did not show more microstructural disruption than pure MCI. Age was positively correlated with cortical fISO (indicating atrophy) and negatively correlated with ODI (indicating neurite complexity) in the total sample ($N = 244$). The strongest age-ODI link was seen in the HC group, and the weakest link was seen in the rMDD and aMCI groups, consistent with frontal-executive and frontostriatal aging models. In contrast, a stepwise relationship was observed between age and fISO: the association was strongest in the HC group, followed by the rMDD group, and then the MCI group. This pattern positions the rMDD group between the HC and MCI groups, suggesting that it is a potential cognitive decline precursor. These results suggest that age-related changes in ODI and fISO could track rMDD progression to dementia. Finally, lower gray matter ODI and higher fISO were correlated with lower cognitive scores across all groups, validating NODDI metrics as neurobiological proxies for cognitive impairment.

NODDI Changes With Age Irrespective of Diagnosis

Our findings are consistent with previous research that has shown age-related increases in fISO and decreases in ODI. Prior studies have shown widespread age-related cortical ODI decreases (24,50), suggesting a decrease in dendritic arborization, and are backed by results of monkey histological studies (13,57) and postmortem human studies (58). Consistent with Nazeri *et al.* (50), we found no evidence of age-related cortical NDI changes. While some studies have reported age-related NDI declines, they usually considered gray and white matter together (59). Others have linked cortical NDI decreases

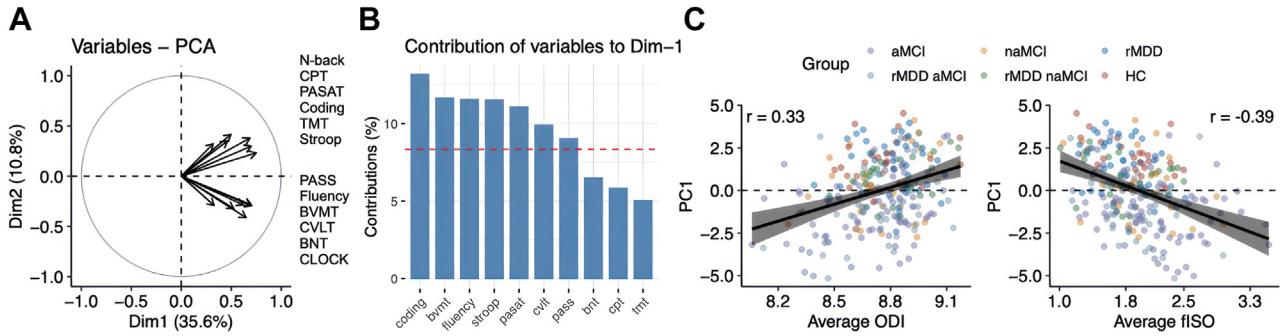

Figure 6. Principal component analysis (PCA) of behavioral variables. Panel **(A)** shows the biplot results of the PCA on cognitive variables. Panel **(B)** shows the 10 cognitive tests that contributed most to the first PCA dimension. The dashed red line indicates the expected average contribution for the variables under a uniform distribution (in this case, 1/12, or 8.3%). Variables exceeding this cutoff can be considered important for contributing to this component. Panel **(C)** shows how average orientation dispersion index (ODI) and isotropic volume fraction (fISO) correlated with the first latent variable (higher PCA scores indicate higher global cognitive performance). Labels on the x-axis are multiplied by 1000. Coding refers to digit symbol substitution, and fluency refers to semantic fluency. aMCI, amnestic MCI; BNT, Boston Naming Test; BVMT, Brief Visuospatial Memory Test; CPT, Continuous Performance Test – Identical Pairs version; CVLT, California Verbal Learning Test; EF, executive function; HC, healthy control; MCI, mild cognitive impairment; naMCI, nonamnestic MCI; PASAT, Paced Auditory Serial Addition Test; PASS, Performance Assessment of Self-Care Skills; rMDD, remitted major depressive disorder; TMT, Trail Making Test.

to advanced age (24) or significant cognitive decline and dementia [e.g., (21,60)]. Generally, NODDI measures, especially ODI, seem to be more sensitive to age-related decline than cortical thickness (50), potentially aiding in detecting early age-related decline (11).

Group-by-Age Effects on ODI

Our second analysis showed that ODI differentiated the HC and naMCI groups from the rMDD group (with or without aMCI). Contrary to our prediction and unlike our fISO results, there was no clear separation of diagnostic groups by microstructure status. Our strongest results were in the bilateral caudate nuclei, where increased age corresponded with a decrease in ODI. This age-related caudate ODI decrease was most evident in the HC and naMCI groups and seemed disrupted in the aMCI and rMDD groups, suggesting abnormal aging. The caudate nucleus, known for its role in motor processes and its disruption in Parkinson's disease, has also been linked to memory (61,62), including procedural and associative memory (63). The age-related decreases in caudate nucleus ODI that we observed may directly affect working memory and cognitive control. We also noted an age-related increase in cerebellum ODI, especially in bilateral crus I, consistent with Nazeri *et al.* (50).

Group-by-Age Effects on fISO

Age-related fISO changes distinguished the HC group from the rMDD group and both of these groups from all MCI groups. While fISO increased with age across the cortex, hippocampus, and caudate nucleus for the entire sample (Figure 3), this link seemed locally disrupted in the MCI groups, primarily in the right caudate nucleus and hippocampus. fISO is associated with neuroinflammation and gliosis presence (64).

In healthy older adults, age-related fISO increases have been reported in various hippocampal subfields such as the dentate gyrus/CA3, CA1, fornix, perirhinal cortex, parahippocampal cortex, and subiculum (65). These fISO effects were attributed to global age-related fISO increases due to ventricular cerebrospinal fluid infiltrating subcortical structures, cell necrosis increases, and general inflammation growth (58). These age-related hippocampal fISO increases were also negatively correlated with delayed recall (58). Because memory impairments typify aMCI, we observed a disruption in the age-fISO relationship in this group, consistent with a prior study (65).

Relationship of NODDI Measures to Global Cognition

Similar to past research on the impact of NODDI measures in aging, we found that global increases in ODI were positively correlated with cognitive performance as represented by the composite PCA score, while the opposite was true for fISO. Importantly, our finding of a negative relationship between global cognition and fISO is consistent with the discovery of a similar relationship between memory measures and hippocampal fISO values by Radhakrishnan *et al.* (65). Collectively, these findings suggest that higher cortical ODI may indicate gray matter health and potentially dendritic arborization, while higher cortical fISO values suggest neuropathology. These results also highlight the utility of using plausible microstructural models in exploring normal and abnormal aging.

Limitations

While an episode of MDD in an older adult increases their risk of MCI and subsequently AD, it is less clear what the risk is for older adults with rMDD. In previous analyses of the same sample of PACt-MD participants, we did not find macrostructural differences in the rMDD and HC groups (10), underscoring the subtlety of the differences between normal aging, rMDD, and MCI. While this new NODDI analysis shows that normal age-related changes in microstructure are disrupted in older people with rMDD or MCI, there are a few limitations to our findings. First, our results are cross-sectional, and thus, we cannot determine causality. Second, in this article, we relied on diagnoses that were established during a research consensus conference by a team of geriatric

psychiatrists and a neuropsychologist using validated diagnostic criteria for MDD and MCI (7,43). However, recent evidence highlights the limitations of these diagnostic labels based on symptoms (i.e., they may not capture underlying biological variability) (66–68). Multivariate machine learning approaches could address this issue by uncovering latent dimensions that link brain and behavior simultaneously. MDD is likely to have multiple etiologies and trajectories. For example, in a recent meta-analysis, we showed that late-onset MDD was associated with more widespread structural abnormalities in regions including visual and attention networks than early-onset MDD (19). Finally, most participants with rMDD were receiving long-term maintenance antidepressants, particularly selective serotonin reuptake inhibitors. The known impact of selective serotonin reuptake inhibitors on BDNF (brain-derived neurotrophic factor) and dendritic complexity could influence measures such as ODI, which is considered a surrogate for dendritic complexity (69). We acknowledge the possible drawbacks of using the NODDI model, which was primarily created for white matter structures rather than for gray matter structures. The small number of HC participants and large number of individuals with naMCI in our study may have skewed the results; future studies should balance sample sizes. Questions exist about the optimal default parallel diffusivity used in the NODDI model, especially for gray matter (70). While some have debated its suitability (71), it is argued that the 1.7 μm^2/ms level may be apt for gray matter due to its lower default parallel diffusivity compared with white matter, but this requires further research. Moreover, the Watson distribution may not be best suited for modeling gray matter. Using NODDI for areas such as the cerebellar cortex, hippocampus, and deep gray matter nuclei, which have unique microstructures, may call for different axial diffusivities. Future work should consider models that are adaptable to various brain area specifics and capable of measuring axial diffusivity directly.

Conclusions

In summary, we showed that age-related changes in gray matter NODDI microstructure measures were associated with diagnoses of rMDD or MCI and with cognitive performance. Moreover, the age-ODI relationship was disrupted in patients with rMDD as it was in those with aMCI, suggesting a potential shared mechanism of risk for dementia related to dendritic complexity. In contrast, the age-fISO relationship was substantially disrupted only in those with MCI, suggesting that atrophy/neurodegeneration is not characteristic of rMDD in late life.

ACKNOWLEDGMENTS AND DISCLOSURES

This work was supported by Brain Canada through the Canada Brain Research Fund with the financial support of Health Canada and the Chagnon Family. JAEA holds a Canada Research Chair Tier II (ID No. CRC-2020-00174) and a Brain and Behavior Research Foundation (BBRF) Young Investigator Award (ID No. 29306). ANV has received grant support from the Canadian Institutes of Health Research (CIHR), the National Institute of Mental Health, the BBRF, Canada Foundation for Innovation, the Centre for Addiction and Mental Health (CAMH) Foundation, and the University of Toronto. AJF has received grant support from the National Institutes of Health (NIH), the Patient-Centered Outcomes Research Institute, the CIHR, Brain Canada, the Ontario Brain Institute, and the Alzheimer's Association. BHM holds and receives support from the Labatt Family Chair in Biology of Depression in Late-Life Adults at the University of Toronto. He currently receives research support from Brain Canada, the CIHR, the CAMH Foundation, the Patient-Centered Outcomes Research Institute, and the NIH. BGP receives research support from the Peter and Shelagh Godsoe Endowed Chair in Late-Life Mental Health, the CAMH Foundation, Discovery Fund, the National Institute on Aging, Brain Canada, the CIHR, the Alzheimer's Drug Discovery Foundation, the Ontario Brain Institute, the Centre for Aging and Brain Health Innovation, the Bright Focus Foundation, the Alzheimer's Society of Canada, the W. Garfield Weston Foundation, the Weston Brain Institute, the Canadian Consortium on Neurodegeneration in Aging, and Genome Canada. CEF receives grant funding from the following sources: Vielight Inc., Hoffman La Roche, the NIH, Brian Canada, the Weston Foundation, and the St. Michael's Hospital Foundation Heather and Eric Donnelly Endowment. TKR has received research support from Brain Canada, the BBRF, BrightFocus Foundation, Canada Foundation for Innovation, Research Canada Chair, the CIHR, the Centre for Aging and Brain Health Innovation, the NIH, the Ontario Ministry of Health and Long-Term Care, the Ontario Ministry of Research and Innovation, and the Weston Brain Institute. PZ was funded by a CIHR postdoctoral fellowship (ID No. CIHR-IRSC:0608000375).

The PACt-MD Study Group comprised the following listed alphabetically by site: Applied Health Research Centre: Kevin E. Thorpe; Baycrest Health Sciences: Tiffany Chow, Linda Mah, Nicolaas P.L.G. Verhoeff; Centre for Addiction and Mental Health (Coordinating Site): Daniel M. Blumberger, Heather Brooks, Angela C. Golas, Ariel Graff-Guerrero, James L. Kennedy, Sanjeev Kumar, Lillian Lourenco, Ashley Melichercik, Benoit H. Mulsant, Shima Ovaysikia, Bruce G. Pollock, Tarek K. Rajji, Erica Vieira, Aristotle N. Voineskos; Queen's University: Christopher R. Bowie; St. Michael's Hospital: Corinne E. Fischer; Sunnybrook Health Sciences Centre: Damien Gallagher, Nathan Herrmann, Krista L. Lanctôt, Mark J. Rapoport; The City College of New York: Marom Bikson; University of California, San Diego: Zafiris J. Daskalakis; University Health Network: Kathleen Bingham, Alastair Flint; University of Pittsburgh: Meryl A. Butters.

Within the past 5 years, BHM has received research support from Capital Solution Design LLC (for software used in a study funded by the CAMH Foundation), Eli Lilly (for medications for an NIH-funded clinical trial), HAPPYneuron (for software used in a study funded by Brain Canada), and Pfizer (for medications for an NIH-funded clinical trial). In addition, he has been an unpaid consultant to Myriad Neuroscience. BGP receives honoraria from the American Geriatrics Society and holds United States Provisional Patent No. 16/490,680 and Canadian Provisional Patent No. 3,054,093 for a cell-based assay and kits for assessing serum anticholinergic activity. TKR received in-kind equipment support for an investigator-initiated study from Magstim and in-kind research accounts from Scientific Brain Training Pro. In 2021 and 2022, TKR participated in an advisory board for Biogen Canada Inc. All other authors report no biomedical financial interests or potential conflicts of interest.

ARTICLE INFORMATION

From the Department of Cognitive Science, Carleton University, Ottawa, Ontario, Canada (JAEA); Campbell Family Mental Health Research Institute, Centre for Addiction and Mental Health, Toronto, Ontario, Canada (JAEA, NR-R, PZ, BHM, BGP, TKR, ANV); Dalla Lana School of Public Health, University of Toronto, Toronto, Ontario, Canada (JAEA); Keenan Research Centre for Biomedical Science, St. Michael's Hospital, Toronto, Ontario, Canada (NR-R, CEF, ANV); Mallinckrodt Institute of Radiology, Washington University School of Medicine, St. Louis, Missouri (AN); Department of Medical Biophysics, University of Toronto, Toronto, Ontario, Canada (JAC); Baycrest Health Sciences, Toronto, Ontario, Canada (JAC, LM); Department of Psychiatry, Temerty Faculty of Medicine, University of Toronto, Toronto, Ontario, Canada (BHM, NH, LM, AJF, CEF, BGP, TKR, ANV); Sunnybrook Health Sciences Centre, Department of Psychiatry, University of Toronto, Toronto, Ontario, Canada (NH); Centre for Mental Health, University Health Network, Toronto, Ontario, Canada (AJF); and Toronto Dementia Research Alliance, University of Toronto, Toronto, Ontario, Canada (TKR).

Address correspondence to Aristotle N. Voineskos, M.D., Ph.D., at aristotle.voineskos@camh.ca.

Received Apr 28, 2023; revised Aug 15, 2023; accepted Aug 27, 2023.
Supplementary material cited in this article is available online at https://doi.org/10.1016/j.bpsgos.2023.08.018.

REFERENCES

1. Jorm AF (2001): History of depression as a risk factor for dementia: An updated review. Aust N Z J Psychiatry 35:776–781.
2. Ownby RL, Crocco E, Acevedo A, John V, Loewenstein D (2006): Depression and risk for Alzheimer disease: Systematic review, meta-analysis, and metaregression analysis. Arch Gen Psychiatry 63:530–538.
3. Herrmann LL, Goodwin GM, Ebmeier KP (2007): The cognitive neuropsychology of depression in the elderly. Psychol Med 37:1693–1702.
4. Koenig AM, DeLozier IJ, Zmuda MD, Marron MM, Begley AE, Anderson SJ, *et al.* (2015): Neuropsychological functioning in the acute and remitted States of late-life depression. J Alzheimers Dis 45:175–185.
5. Sheline YI, Barch DM, Garcia K, Gersing K, Pieper C, Welsh-Bohmer K, *et al.* (2006): Cognitive function in late life depression: Relationships to depression severity, cerebrovascular risk factors and processing speed. Biol Psychiatry 60:58–65.
6. Dybedal GS, Tanum L, Sundet K, Gaarden TL, Bjølseth TM (2013): Neuropsychological functioning in late-life depression. Front Psychol 4:381.
7. Rashidi-Ranjbar N, Miranda D, Butters MA, Mulsant BH, Voineskos AN (2020): Evidence for structural and functional alterations of frontal-executive and corticolimbic circuits in late-life depression and relationship to mild cognitive impairment and dementia: A systematic review. Front Neurosci 14:253.
8. Linnemann C, Lang UE (2020): Pathways connecting late-life depression and dementia. Front Pharmacol 11:279.
9. Cipriani G, Lucetti C, Carlesi C, Danti S, Nuti A (2015): Depression and dementia. A review. Eur Geriatr Med 6:479–486.
10. Rashidi-Ranjbar N, Rajji TK, Kumar S, Herrmann N, Mah L, Flint AJ, *et al.* (2020): Frontal-executive and corticolimbic structural brain circuitry in older people with remitted depression, mild cognitive impairment, Alzheimer's dementia, and normal cognition. Neuropsychopharmacology 45:1567–1578.
11. Nazeri A, Schifani C, Anderson JAE, Ameis SH, Voineskos AN (2020): In vivo imaging of gray matter microstructure in major psychiatric disorders: Opportunities for clinical translation. Biol Psychiatry Cogn Neurosci Neuroimaging 5:855–864.
12. Bloss E, Morrison J, Hof P, Dickstein D (2011): Influence of aging and neurodegeneration on dendritic spine morphology. Transl Neurosci 2:49–60.
13. Dickstein DL, Weaver CM, Luebke JI, Hof PR (2013): Dendritic spine changes associated with normal aging. Neuroscience 251:21–32.
14. Fogarty MJ, Mu EWH, Noakes PG, Lavidis NA, Bellingham MC (2016): Marked changes in dendritic structure and spine density precede significant neuronal death in vulnerable cortical pyramidal neuron populations in the SOD1(G93A) mouse model of amyotrophic lateral sclerosis. Acta Neuropathol Commun 4:77.
15. Pannese E (2011): Morphological changes in nerve cells during normal aging. Brain Struct Funct 216:85–89.
16. Teissier T, Boulanger E, Deramecourt V (2020): Normal ageing of the brain: Histological and biological aspects. Rev Neurol (Paris) 176:649–660.
17. Boccia M, Acierno M, Piccardi L (2015): Neuroanatomy of Alzheimer's disease and late-life depression: A coordinate-based meta-analysis of MRI studies. J Alzheimers Dis 46:963–970.
18. Sexton CE, Mackay CE, Ebmeier KP (2013): A systematic review and meta-analysis of magnetic resonance imaging studies in late-life depression. Am J Geriatr Psychiatry 21:184–195.
19. Zhukovsky P, Anderson JAE, Coughlan G, Mulsant BH, Cipriani A, Voineskos AN (2021): Coordinate-based network mapping of brain structure in major depressive disorder in younger and older adults: A systematic review and meta-analysis. Am J Psychiatry 178:1119–1128.
20. Rashidi-Ranjbar N, Rajji TK, Hawco C, Kumar S, Herrmann N, Mah L, *et al.* (2023): Association of functional connectivity of the executive control network or default mode network with cognitive impairment in older adults with remitted major depressive disorder or mild cognitive impairment. Neuropsychopharmacology 48:468–477.
21. Vogt NM, Hunt JF, Adluru N, Dean DC, Johnson SC, Asthana S, *et al.* (2020): Cortical microstructural alterations in mild cognitive impairment and Alzheimer's disease dementia. Cereb Cortex 30:2948–2960.
22. Stauffer E-M, Bethlehem RAI, Warrier V, Murray GK, Romero-Garcia R, Seidlitz J, Bullmore ET (2021): Grey and white matter microstructure is associated with polygenic risk for schizophrenia. Mol Psychiatry 26:7709–7718.
23. Elliott LT, Sharp K, Alfaro-Almagro F, Shi S, Miller KL, Douaud G, *et al.* (2018): Genome-wide association studies of brain imaging phenotypes in UK Biobank. Nature 562:210–216.
24. Gozdas E, Fingerhut H, Dacorro L, Bruno JL, Hosseini SMH (2021): Neurite imaging reveals widespread alterations in gray and white matter neurite morphology in healthy aging and amnestic mild cognitive impairment. Cereb Cortex 31:5570–5578.
25. Zhang H, Schneider T, Wheeler-Kingshott CA, Alexander DC (2012): NODDI: Practical in vivo neurite orientation dispersion and density imaging of the human brain. Neuroimage 61:1000–1016.
26. Chad JA, Pasternak O, Salat DH, Chen JJ (2018): Re-examining age-related differences in white matter microstructure with free-water corrected diffusion tensor imaging. Neurobiol Aging 71:161–170.
27. Andersen KW, Lasič S, Lundell H, Nilsson M, Topgaard D, Sellebjerg F, *et al.* (2020): Disentangling white-matter damage from physiological fibre orientation dispersion in multiple sclerosis. Brain Commun 2:fcaa077.
28. Anderson JAE, Schifani C, Nazeri A, Voineskos AN (2021): In vivo cortical microstructure -A proxy for tauopathy & cognitive impairment. medRxiv. https://doi.org/10.1101/2021.03.26.2125435.
29. Mak E, Bethlehem RAI, Romero-Garcia R, Cervenka S, Rittman T, Gabel S, *et al.* (2018): In vivo coupling of tau pathology and cortical thinning in Alzheimer's disease. Alzheimers Dement (Amst) 10:678–687.
30. Rajji TK, Bowie CR, Herrmann N, Pollock BG, Bikson M, Blumberger DM, *et al.* (2020): Design and Rationale of the PACt-MD Randomized Clinical Trial: Prevention of Alzheimer's dementia with cognitive remediation plus transcranial direct current stimulation in Mild cognitive impairment and Depression. J Alzheimers Dis 76:733–751.
31. Kirchner WK (1958): Age differences in short-term retention of rapidly changing information. J Exp Psychol 55:352–358.
32. Beck LH, Bransome ED, Mirsky AF, Rosvold HE, Sarason I (1956): A continuous performance test of brain damage. J Consult Psychol 20:343–350.
33. Gronwall DM (1977): Paced auditory serial-addition task: A measure of recovery from concussion. Percept Mot Skills 44:367–373.
34. Jaeger J (2018): Digit symbol substitution test: The case for sensitivity over specificity in neuropsychological testing. J Clin Psychopharmacol 38:513–519.
35. Reitan RM (1956): Trail Making Test. Manual for Administration, Scoring, and Interpretation. Indianapolis: Indiana University Press.
36. Stroop JR (1935): Studies of interference in serial verbal reactions. J Exp Psychol 18:643–662.
37. Holm MB, Rogers JC, Hemphill-Pearson B (2008): The Performance Assessment of Self-Care Skills (PASS). Ini: Hemphill-Pearson BJ. In: Assessments in Occupational Therapy Mental Health. 2nd ed. Thorofare, New Jersey: SLACK, 101–110.
38. Bousfield WA, Sedgewick CH, Cohen BH (1954): Certain temporal characteristics of the recall of verbal associates. Am J Psychol 67:111–118.
39. Benedict RHB, Schretlen D, Groninger L, Dobraski M, Shpritz B (1996): Revision of the Brief Visuospatial Memory Test: Studies of normal performance, reliability, and validity. Psychol Assess 8:145–153.
40. Delis DC, Kramer JH, Kaplan E, Ober BA (2016): California Verbal Learning Test, 2nd ed. PsycTESTS Dataset. Washington: American Psychological Association.

41. Kaplan E, Goodglass H, Weintraub S (2001): Boston Naming Test Available at: https://osf.io/vy8gh/download. Accessed August 18, 2022.
42. Shulman KI (2000): Clock-drawing: Is it the ideal cognitive screening test? Int J Geriatr Psychiatry 15:548–561.
43. Weinstein AM, Gujral S, Butters MA, Bowie CR, Fischer CE, Flint AJ, *et al.* (2022): Diagnostic precision in the detection of mild cognitive impairment: A comparison of two approaches. Am J Geriatr Psychiatry 30:54–64.
44. Petersen RC (2004): Mild cognitive impairment as a diagnostic entity. J Intern Med 256:183–194.
45. Andersson JLR, Sotiropoulos SN (2016): An integrated approach to correction for off-resonance effects and subject movement in diffusion MR imaging. Neuroimage 125:1063–1078.
46. Jenkinson M, Beckmann CF, Behrens TEJ, Woolrich MW, Smith SM (2012). FSL. Neuroimage 62:782–790.
47. Harms RL, Fritz FJ, Tobisch A, Goebel R, Roebroeck A (2017): Robust and fast nonlinear optimization of diffusion MRI microstructure models. Neuroimage 155:82–96.
48. Harms RL, Roebroeck A (2018): Robust and fast Markov chain Monte Carlo sampling of diffusion MRI microstructure models. Front Neuroinform 12:97.
49. Ball G, Srinivasan L, Aljabar P, Counsell SJ, Durighel G, Hajnal JV, *et al.* (2013): Development of cortical microstructure in the preterm human brain. Proc Natl Acad Sci U S A 110:9541–9546.
50. Nazeri A, Chakravarty MM, Rotenberg DJ, Rajji TK, Rathi Y, Michailovich OV, Voineskos AN (2015): Functional consequences of neurite orientation dispersion and density in humans across the adult lifespan. J Neurosci 35:1753–1762.
51. Nazeri A, Mulsant BH, Rajji TK, Levesque ML, Pipitone J, Stefanik L, *et al.* (2017): Gray matter neuritic microstructure deficits in schizophrenia and bipolar disorder. Biol Psychiatry 82:726–736.
52. Smith SM, Jenkinson M, Johansen-Berg H, Rueckert D, Nichols TE, Mackay CE, *et al.* (2006): Tract-based spatial statistics: Voxelwise analysis of multi-subject diffusion data. Neuroimage 31:1487–1505.
53. McIntosh AR, Lobaugh NJ (2004): Partial least squares analysis of neuroimaging data: Applications and advances. Neuroimage 23(suppl 1):S250–S263.
54. Krishnan A, Williams LJ, McIntosh AR, Abdi H (2011): Partial least squares (PLS) methods for neuroimaging: A tutorial and review. Neuroimage 56:455–475.
55. Bastiani M, Cottaar M, Fitzgibbon SP, Suri S, Alfaro-Almagro F, Sotiropoulos SN, *et al.* (2019): Automated quality control for within and between studies diffusion MRI data using a non-parametric framework for movement and distortion correction. Neuroimage 184:801–812.
56. Tournier JD, Smith R, Raffelt D, Tabbara R, Dhollander T, Pietsch M, *et al.* (2019): MRtrix3: A fast, flexible and open software framework for medical image processing and visualisation. Neuroimage 202:116137.
57. Duan H, Wearne SL, Rocher AB, Macedo A, Morrison JH, Hof PR (2003): Age-related dendritic and spine changes in corticocortically projecting neurons in macaque monkeys. Cereb Cortex 13:950–961.
58. Anderson B, Rutledge V (1996): Age and hemisphere effects on dendritic structure. Brain 119:1983–1990.
59. Ota M, Sato N, Maikusa N, Sone D, Matsuda H, Kunugi H (2017): Whole brain analyses of age-related microstructural changes quantified using different diffusional magnetic resonance imaging methods. Jpn J Radiol 35:584–589.
60. Parker TD, Slattery CF, Zhang J, Nicholas JM, Paterson RW, Foulkes AJM, *et al.* (2018): Cortical microstructure in young onset Alzheimer's disease using neurite orientation dispersion and density imaging. Hum Brain Mapp 39:3005–3017.
61. White NM (2009): Some highlights of research on the effects of caudate nucleus lesions over the past 200 years. Behav Brain Res 199:3–23.
62. Foerde K, Shohamy D (2011): The role of the basal ganglia in learning and memory: Insight from Parkinson's disease. Neurobiol Learn Mem 96:624–636.
63. Bauer E, Toepper M, Gebhardt H, Gallhofer B, Sammer G (2015): The significance of caudate volume for age-related associative memory decline. Brain Res 1622:137–148.
64. Pfefferbaum A, Adalsteinsson E, Rohlfing T, Sullivan EV (2009): MRI estimates of brain iron concentration in normal aging: Comparison of field-dependent (FDRI) and phase (SWI) methods. Neuroimage 47:493–500.
65. Radhakrishnan H, Stark SM, Stark CEL (2020): Microstructural alterations in hippocampal subfields mediate age-related memory decline in humans. Front Aging Neurosci 12:94.
66. Voineskos AN, Jacobs GR, Ameis SH (2020): Neuroimaging heterogeneity in psychosis: Neurobiological underpinnings and opportunities for prognostic and therapeutic innovation. Biol Psychiatry 88:95–102.
67. Jacobs GR, Voineskos AN, Hawco C, Stefanik L, Forde NJ, Dickie EW, *et al.* (2021): Integration of brain and behavior measures for identification of data-driven groups cutting across children with ASD, ADHD, or OCD. Neuropsychopharmacology 46:643–653.
68. Fried EI (2017): The 52 symptoms of major depression: Lack of content overlap among seven common depression scales. J Affect Disord 208:191–197.
69. Duman RS, Deyama S, Fogaça MV (2021): Role of BDNF in the pathophysiology and treatment of depression: Activity-dependent effects distinguish rapid-acting antidepressants. Eur J Neurosci 53:126–139.
70. Guerrero JM, Adluru N, Bendlin BB, Goldsmith HH, Schaefer SM, Davidson RJ, *et al.* (2019): Optimizing the intrinsic parallel diffusivity in NODDI: An extensive empirical evaluation. PLoS One 14:e0217118.
71. Howard AF, Cottaar M, Drakesmith M, Fan Q, Huang SY, Jones DK, *et al.* (2022): Estimating axial diffusivity in the NODDI model. Neuroimage 262:119535.